NOTES AND CORRESPONDENCE

Adjoint-Method Retrievals of Low-Altitude Wind Fields from Single-Doppler Reflectivity and Radial-Wind Data

QIN XU AND CHONG-JIAN QIU*

Cooperative Institute for Mesoscale Meteorological Studies, University of Oklahoma/NOAA, Norman, Oklahoma

8 June 1994 and 30 March 1995

ABSTRACT

The simple adjoint (SA) method is extended to use both the reflectivity equation and the radial-wind equation to retrieve the low-altitude horizontal wind field from single-Doppler reflectivity and radial-wind data. Three extended methods are proposed. The extended method A uses the reflectivity equation and radial-wind equation simultaneously. The extended method B (or method C) uses the reflectivity equation and radial-wind equation alternately with the velocity retrieved from the reflectivity (or radial wind) data first. The first-step retrieved wind is then used to estimate the time-mean residual forcing (or source) term in the radial-wind (or reflectivity) equation, and this estimated forcing (or source) is used as a weak constraint in the second-step retrieval from the radial-wind (or reflectivity) data. The retrieval is expected to be maximally improved when the procedure goes to the third step (and beyond). Tested with the Doppler radar data measured during the Phoenix II field experiment, all three extended methods are found to be better than the previous SA method based on a single (reflectivity or radial wind) equation. Among the three extended methods, method C is found to be slightly better than method A, but slightly worse than method B.

1. Introduction

A simple adjoint (SA) method was developed by Qiu and Xu (1992, henceforth referred to as QX92) for retrieving the time-mean wind field from the movements of reflectivity patterns measured through a sequence of single-Doppler radar scans. The SA method has been recently upgraded and tested with the Phoenix II data for retrieving the low-altitude time-mean (or running mean) winds from either single-Doppler reflectivity or radial wind (Xu et al. 1994a,b, henceforth referred to as XQY94a,b). The test results were very encouraging, but there is still room for further improvements. Since the reflectivity and radial wind measured by a Doppler radar contain independent information for the flow advection, a combined use of the reflectivity equation and the radial-wind equation may improve the velocity retrieval and/or make the retrieval more reliable. This problem, however, has not been previously examined with the SA method. To explore the possible merits for a combined use of the reflectivity equation and the radial-wind equation, the SA method is extended with three different approaches. The extended methods and their adjoint formulations are derived in section 2. The experimental designs are described in section 3. The extended methods are tested with the Phoenix II data in section 4, and the results are positive. Conclusions follow in section 5.

2. Method description

To make use of both the reflectivity equation and the radial-wind equation, the SA method needs to be extended. The extensions can be made with the following different approaches.

A: Use the reflectivity equation and radial-wind equation simultaneously.

B: Use the reflectivity equation and radial-wind equation alternately, and start with the reflectivity data first. The retrieved velocity is then substituted into the radial-wind equation to estimate the time-mean residual forcing term. This estimated forcing is used as a weak constraint in the second-step retrieval from the radial-wind data. A similar alternate procedure can go to the third step and beyond.

C: Similar to method B, but start with the radial-wind data first.

Before we describe the detailed methods, we need to show the simplified reflectivity equation and radial-wind equation in the next subsection.

* Permanent affiliation: Department of Atmospheric Science, Lanzhou University, Lanzhou City, People's Republic of China.

Corresponding author address: Prof. Qin Xu, CIMMS, University of Oklahoma, Room 1110, 100 East Boyd, Norman, OK 73019-0628.

TABLE 1. Mean absolute values (10^{-3} s^{-1}) of terms in Eq. (2.1).

Data	$\{\lvert\partial_t\eta\rvert\}$	$\{\lvert\mathbf{v}_m\cdot\nabla_H\eta\rvert\}$	$\{\lvert\kappa\nabla_H^2\eta\rvert\}$	$\{\lvert S_m\rvert\}$	$\{\lvert S'\rvert\}$
I	6.91	7.29	0.65	3.26	2.32
II	6.46	6.91	0.69	2.30	1.30
III	5.62	7.03	0.62	3.59	2.06
Average	6.33	7.08	0.65	3.05	1.89
Relative magnitude	89%	100%	9%	43%	27%

a. Simplified equations

The reflectivity advection equation in the cylindrical coordinates (r, α, z) (centered at the single-Doppler radar C as shown in Fig. 1 of XQY94a) on the low altitudes of the radar scans has the following form:

$$\partial_t\eta + v_{rm}\partial_r\eta + \left(\frac{v_{\alpha m}}{r}\right)\partial_\alpha\eta - \kappa_\eta\nabla_H^2\eta = S_m + S' \approx S_m, \tag{2.1}$$

where η is the (logarithmic) reflectivity in nondimensional unit dB [that is, $\eta \equiv 10\log(B/B_0)$ and B/B_0 is the nondimensional reflectivity scaled by a reference value B_0]; ∇_H^2 is the horizontal Laplacian in cylindrical coordinates; and κ_η is the coefficient of horizontal eddy diffusion for reflectivity, which is assumed to be an unknown constant and needs to be retrieved. Here $(\ )_m \equiv \tau^{-1}\int_0^\tau(\ )dt$ denotes the time mean (or running mean), $\tau \equiv N\Delta\tau$ is the averaging period covering $N + 1$ sequential radar scans, and $\Delta\tau$ is the time elapsed for one scan. The horizontal vector wind $\mathbf{v} \equiv (v_r, v_\alpha)$ is partitioned into a time-mean part $\mathbf{v}_m \equiv (v_{rm}, v_{\alpha m})$ and a temporal fluctuation part $\mathbf{v}' \equiv (v_r', v_\alpha')$. The residual source term $S \equiv S_0 + \nu\partial_z^2\eta - (w - w_0)\partial_z\eta - v_r'\partial_r\eta - (v_\alpha'/r)\partial_\alpha\eta$ is also partitioned into a time-mean part S_m and a temporal fluctuation part S', where ν is the coefficient of vertical eddy diffusion, w_0 is the terminal velocity of aluminum chaff (or hydrometeor) relative to the air, and S_0 is an unknown source term (which may be negligible for chaff reflectivity but not for hydrometeor reflectivity). Here, (2.1) is similar to (3.3) of XQY94a except for the unknown source term. Although S' is not very small (see Table 1), this term has to be neglected. Otherwise, as explained in XQY94b, the total number of unknowns will be greater than the number of the discretized model equations plus the number of data points. Nevertheless, the time-mean part of the unknown source can be retrieved. The boundary and initial conditions for (2.1) are

$$\eta(t, r, \alpha) = \eta_{ob}(t, r, \alpha) \tag{2.2}$$

at the boundary of domain Ω,

$$\eta(0, r, \alpha) = \eta_{ob}(0, r, \alpha), \tag{2.3}$$

where $(\ )_{ob}$ represents the observed value of $(\ )$. Equation (2.1) with (2.2) and (2.3) provides a strong constraint (Sasaki 1970) for the extended SA method.

By similarly applying the time-mean partition to the radial-wind equation, we obtain

$$\partial_t v_r + v_{rm}\partial_r v_r + \frac{v_{\alpha m}}{r}\partial_\alpha v_r - \frac{v_{\alpha m}^2}{r} - \kappa_v\nabla_H^2 v_r = F_m + F' \approx F_m, \tag{2.4}$$

where the radial wind v_r (from radar C) is used as a "tracer" field, κ_v is the coefficient of horizontal eddy diffusion for radial velocity, and F_m and F' are the time-mean part and temporal fluctuation part of the unknown forcing, respectively [mainly the pressure gradient and vertical advection terms, see (2.1) and (2.2) of XQY94b]. Here F' has to be neglected due to the same reason as explained for S', though this term is not very small (see Table 2). Since the data were collected at very low elevation angles (see section 3a), the observed radial winds (along the radar beam) are assumed to be horizontal. The boundary and initial conditions are

$$v_r(t, r, \alpha) = v_{rob}(t, r, \alpha) \tag{2.5}$$

at the boundary of domain Ω,

$$v_r(0, r, \alpha) = v_{rob}(0, r, \alpha). \tag{2.6}$$

Equation (2.4) with (2.5) and (2.6) provides another strong constraint for the extended SA method.

TABLE 2. Mean absolute values (10^{-3} m s^{-2}) of terms in Eq. (2.4).

Data	$\{\lvert\partial_t v_r\rvert\}$	$\{\lvert\mathbf{v}_m\cdot\nabla_H v_r\rvert\}$	$\{\lvert v_{\alpha m}^2/r\rvert\}$	$\{\lvert\kappa\nabla_H^2 v_r\rvert\}$	$\{\lvert F_m\rvert\}$	$\{\lvert F'\rvert\}$
I	3.27	3.94	1.60	0.35	2.13	1.30
II	2.57	3.80	1.34	0.37	1.45	0.50
III	2.70	3.25	1.74	0.36	2.58	1.13
Average	2.85	3.66	1.56	0.36	2.05	0.98
Relative magnitude	78%	100%	43%	10%	56%	27%

b. Extended methods

The extended method A uses the reflectivity equation (2.1) and the radial-wind equation (2.4) simultaneously, and the goal is to find the best estimates of ($\mathbf{v}_m$, S_m, F_m, κ_η, κ_v) over a period τ that give the best "predictions" of η and v_r in terms of minimizing the following cost function:

$$J \equiv \{\{P_1\Delta_\eta^2 + P_2\Delta_v^2 + P_3\Delta_m^2 + P_4 d_m^2 + P_5\zeta_m^2\}\}_m$$
$$\equiv J_1 + J_2 + J_3 + J_4 + J_5, \tag{2.7}$$

where

$$\Delta_\eta \equiv \eta - \eta_{\text{ob}}, \quad \Delta_v \equiv v_r - v_{\text{rob}}, \quad \Delta_m \equiv v_{rm} - v_{\text{rob}m},$$
$$d_m \equiv \nabla_H \cdot \mathbf{v}_m, \quad \zeta_m \equiv \mathbf{k} \cdot \nabla_H \times \mathbf{v}_m,$$

where ∇_H is the horizontal gradient operator in cylindrical coordinates, $(\ )_m \equiv \tau^{-1}\int_0^\tau (\ )dt$ is the time-mean (or running mean) operator as defined earlier, $(\ )_{\text{ob}m}$ is the time-mean of the observed value of $(\ )$, $\{\{(\ )\}\} \equiv \Omega^{-1}\iint (\ )d\Omega$ is the area-mean operator over the retrieval domain, P_1 is a nondimensional weight, P_2 and P_3 are dimensional weights (m^{-2} s^2), and P_4 and P_5 are dimensional weights (s^2). Here η is "predicted" by (2.1)–(2.3) and v_r is predicted by (2.4)–(2.6). As explained in QX92, the period τ should be long enough to cover the necessary multiple time levels of measurement but not be too long to violate the quasi-steady assumption over the period τ. The first part, J_1, of the cost function constrains the difference between the reflectivity prediction η and observation η_{ob}, while the second part, J_2, constrains the difference between the radial-wind prediction v_r and observation v_{rob}. The third part, J_3, gives a weak constraint (Sasaki 1970) on the difference between the retrieved and observed time-mean radial winds. Note that J_3 is a weak constraint for the retrieved time-mean radial wind, while J_2 is a strong constraint for the predicted radial wind (tracer), so J_3 plays a different role than J_2 in the cost function. As explained in XQY94b, using J_3 is better than directly using $v_{\text{rob}m}$ (to replace v_{rm}) in the model equations and their adjoint equations. The last two parts, J_4 and J_5, impose weak divergence and vorticity constraints on the retrieved horizontal wind field. These two constraints are essentially smoothness constraints. Other forms of smoothness constraints have also been tried and tested (not shown), but the retrievals are improved not as much as obtained by using J_4 and J_5.

By using the similar derivation as in appendix B of XQY94a, one can verify that the components of the gradient of J are given by

$$\frac{\partial J}{\partial v_{rm}} = \left(\eta^*\partial_r\eta + v_r^*\partial_r v_r + 2P_3\Delta_m - 2P_4\partial_r d_m + 2P_5\frac{\partial_\alpha\zeta_m}{r}\right)_m \frac{\Delta\Omega}{\Omega},$$

$$\frac{\partial J}{\partial v_{\alpha m}} = [\eta^*\partial_\alpha\eta + v_r^*(\partial_\alpha v_r - 2v_{\alpha m}) - 2P_4\partial_\alpha d_m - 2P_5 r\partial_r\zeta_m]_m \frac{\Delta\Omega}{r\Omega},$$

$$\frac{\partial J}{\partial S_m} = -(\eta^*)_m\frac{\Delta\Omega}{\Omega}, \quad \frac{\partial J}{\partial F_m} = -(v_r^*)_m\frac{\Delta\Omega}{\Omega},$$

$$\frac{\partial J}{\partial \kappa_\eta} = -\{\{\eta^*\nabla_H^2\eta\}\}_m,$$

$$\frac{\partial J}{\partial \kappa_v} = -\{\{v_r^*\nabla_H^2 v_r\}\}_m, \tag{2.8}$$

where $\Delta\Omega \equiv r\Delta r\Delta\alpha$ is the area represented by a grid point in the cylindrical coordinates, and η^* and v_r^* are the solutions of the associated adjoint equations (not shown). The numerical code is designed carefully to ensure the conjugate property between the discretized operator and adjoint operator (Lewis and Derber 1985; Talagrand and Courtier 1987). As in XQY94a,b, the standard conjugate gradient algorithm (UMCGG in the IMSL Math Library) is used together with the cost function J in (2.7) and its gradients in (2.8) to search the minimum of J.

The extended method B uses the reflectivity equation and radial-wind equation alternately in the following sequence. First, the velocity is retrieved by using the reflectivity equation (2.1), similarly to that in XQY94a. Since this first step uses only the reflectivity equation (2.1), the cost function is given by (2.7) with $P_2 = 0$, and the gradient terms are given by (2.8) with $P_2 = v_r^* = 0$. Then, the first-step retrieved velocity is substituted into the radial-wind equation (2.4) to estimate the time-mean forcing term. This estimated forcing, denoted by F_{me}, is used to constrain the forcing term F_m in the second-step retrieval, while the first-step retrieved velocity is used as the initial guess. Thus, in this second step, the cost function is given by (2.7) with J_1 replaced by

$$J_6 \equiv \{\{P_6(F_m - F_{me})^2\}\}, \tag{2.9}$$

where P_6 is the weight and J_6 imposes a weak constraint on the forcing F_m. Note that $\delta J_6 = \langle 2P_6(F_m - F_{me}), \delta F_m\rangle$, so the gradient terms in (2.8) need to be modified with $P_1 = \eta^* = 0$ and $\partial J/\partial F_m = [2P_6(F_m - F_{me}) - (v_r^*)_m](\Delta\Omega/\Omega)$.

The second-step retrieved velocity is used as the initial guess for the third step retrieval from the reflectivity data, and substituted into the reflectivity equation (2.1) to estimate the time-mean source term. The estimated source term, denoted by S_{me}, is used to constrain the source term S_m. Thus, in the third step, the cost function is given by (2.7) with J_2 replaced by

$$J_7 \equiv \{\{P_7(S_m - S_{me})^2\}\}, \tag{2.10}$$

where P_7 is the weight and J_7 imposes a weak constraint on the source S_m. Note that $\delta J_7 = \langle 2P_7(S_m - S_{me}),$

$\delta S_m\rangle$, so the gradient terms in (2.8) need to be modified with $P_2 = v_r^* = 0$ and $\partial J/\partial S_m = [2P_7(S_m - S_{me}) - (\eta^*)_m](\Delta\Omega/\Omega)$. The fourth step can be performed similarly to the second step, and so on. But, as indicated by our numerical results, the retrieval will hardly be improved after the third step.

The extended method C is similar to the above method B, but the velocity is retrieved first from the radial-wind data by using the radial-wind equation (2.4), as in XQY94b. In this step, the cost function is given by (2.7) with $P_1 = 0$, and the gradient terms are given by (2.8) with $P_1 = \eta^* = 0$. The second and third steps can be performed similarly to the third and fourth steps, respectively, in the above method B. Again, as indicated by our numerical results, the retrieval will hardly be improved after the third step.

Before proceeding to the next section, it is worth mentioning the problem with scaling, ellipticity of the supersurface of the cost function, and convergence rate of iteration (Moore 1991; XQY94b). If the conventional units (s^{-1}, m s^{-2}) are used for (S_m, F_m), then $\partial J/\partial S_m$ and $\partial J/\partial F_m$ will be much larger than the remaining four gradient components in (2.8). This means that the supersurface of the cost function is highly elliptical and the above descent algorithm may hardly converge unless S_m and F_m are properly rescaled. The proper scale for S_m can be estimated from the observed mean absolute value of the first term $\partial_t\eta$ in (2.1), which is about 0.006 s^{-1} (as shown in Table 1). The proper scale for F_m can be estimated from the observed mean absolute value of the first term $\partial_t v_r$ in (2.4), which is about 0.003 m s^{-2} (as shown in Table 2). With these scales, $\partial J/\partial S_m$ and $\partial J/\partial F_m$ have about the same nondimensional magnitudes as the remaining gradient components in (2.8), so the supersurface of the cost function becomes locally close to spherical or at least less elliptical and the descent algorithm converges rapidly.

3. Data and experiment design

a. Data and equation errors

The Phoenix II experiment data collected by two X-band Doppler radars (i.e., radar C and radar D as shown in Fig. 1 of XQY94a) on 17 and 22 June 1984 are used in this study. Gridded data are obtained, by using the Cressman interpolation, from the following three raw datasets:

set I covers the period of 1437:26–1443:58 UTC 22 June 1984;

set II covers the period of 1318:32–1324:48 UTC 22 June 1984;

set III covers the period of 1237:28–1243:58 UTC 17 June 1984.

The grid resolutions are $(\Delta r, \Delta\alpha) = (112$ m, $1°)$ in the cylindrical coordinates (centered at radar C), and time resolution is $\Delta\tau = 130$ s. The detailed procedures of data processing are described in XQY94a,b.

From the above three datasets, the magnitudes of the terms in (2.1) and (2.4) are computed in Tables 1 and 2, respectively, where

$$\{|(\quad)|\} \equiv \frac{\Sigma \int_0^\tau |(\quad)|\, dt}{\tau \times 28 \times 26} \tag{3.1}$$

is the mean absolute value of ( ) with $\tau = 2\Delta\tau$ (=260 s). The dual-Doppler observed wind field $\mathbf{v}_{ob}$ and retrieved κ_η (ranged from 110.2 to 120.9 $m^2\ s^{-1}$) are used for the computations in Table 1. Since S' is obtained by substituting $\mathbf{v}_{ob}$ and retrieved κ_η into (2.1), the estimated value of S' should actually contain not only the equation error of (2.1) (with S' neglected) but also the data error. The terms in Table 2 are estimated similarly to those in Table 1, except the retrieved κ_v (ranged from 104.2 to 109.2 $m^2\ s^{-1}$) is used. The estimated value of F' contains both the data error and equation error of (2.4) (with F' neglected).

As shown in Tables 1 and 2, the local time derivative term and advection term are the largest. The magnitude of the time-mean residual source term S_m is only 43% of the advection term in (2.1) but is significantly larger than the error term S'. The magnitude of the time-mean residual forcing term F_m is only 56% of the magnitude of the advection term in (2.4) but is still significantly larger than the error term F'. The centrifugal term $v_{\alpha m}^2/r$ is significant, but this does not necessarily mean that the explicit form of this term is important. As shown in XQY94b, the centrifugal term can be retrieved implicitly as a part of the residual term. The viscous terms are relatively small, but these terms will become relatively large if short-wave noise is not properly filtered by the Cressman interpolation. As shown by the results in Table 1 of XQY94a (and also confirmed by the results in this paper, but not shown), including the viscous terms and retrieving κ_η and κ_v can suppress short-wave noise and improve the wind retrieval.

b. Experiment design

All the experiments use three time levels of data and the retrieving period covers two time intervals of observations; that is, $\tau \equiv N\Delta\tau = 2 \times 130$ s. This retrieving period is in the optimal range in terms of gaining accuracy without much loss of time resolution. The finite-difference scheme is used with $(\Delta r, \Delta\alpha) = (112$ m, $1°)$, and the computational time step is $\Delta t = 6.5$ s. All the retrievals are computed by 60 steps of iteration. It is found that the retrievals are improved significantly in the first 50 steps of iteration but cannot be further improved and actually become slightly worse as the number of iterations goes beyond 100 steps, although the cost function J converges continuously toward the

TABLE 3. Results of experiments (with $\tau = 2 \times 130$ s and $\mu = 0.01$).

Experiment	μ_η	μ_v	k_d (s^2)	k_ζ (s^2)	Source	μ_f	μ_s	RRE (%) v_m	S_m	F_m
E0A	1	1	0	0	no	0	0	44.1		
E0B	1	0	0	0	no	0	0	46.3		
E0C	0	1	0	0	no	0	0	58.2		
E1A	1	1	0	0	yes	0	0	36.6	87.9	74.3
E1B	1	0	0	0	yes	0	0	42.1	90.2	
E1B2	0	1	0	0	yes	10^{-4}	0	37.2		82.8
E1B3	1	0	0	0	yes	10^{-4}	10^{-4}	35.6	86.1	
E1C	0	1	0	0	yes	0	0	50.0		96.8
E1C2	1	0	0	0	yes	0	10^{-4}	40.1	83.7	
E1C3	0	1	0	0	yes	10^{-4}	10^{-4}	35.6		86.1
E2A	1	1	100	100	yes	0	0	25.6	85.5	61.7
E2B	1	0	100	100	yes	0	0	26.6	82.7	
E2B2	0	1	100	100	yes	10^{-4}	0	22.9		50.9
E2B3	1	0	100	100	yes	10^{-4}	10^{-4}	21.9	52.0	
E2C	0	1	100	100	yes	0	0	34.9		79.9
E2C2	1	0	100	100	yes	0	10^{-4}	24.4	75.0	
E2C3	0	1	100	100	yes	10^{-4}	10^{-4}	22.1		48.9

minimum. As shown in Xu and Qiu (1994), this feature is common and related to the fact that the data and the equation are not error free.

The seven weights in (2.7), (2.9), and (2.10) are chosen to have the following forms:

$$P_1 = \frac{\mu_\eta P_0}{\sigma_\eta^2},$$

$$P_2 = \frac{\mu_v P_0}{\sigma_v^2},$$

$$P_3 = \frac{\mu P_m}{\sigma_v^2} \quad (\mu = 0.01),$$

$$P_4 = k_d P_m \quad (k_d = 100 \text{ s}^2),$$

$$P_5 = k_\zeta P_m \quad (k_\zeta = 100 \text{ s}^2),$$

$$P_6 = \frac{\mu_f P_m}{\sigma_f^2} \quad (\mu_f = 10^{-4}),$$

$$P_7 = \frac{\mu_s P_m}{\sigma_s^2} \quad (\mu_s = 10^{-4}), \tag{3.2}$$

where $P_0 \equiv 0.5[\tau(t + \Delta t)^{-1}]^{1/2}$ with $P_m \equiv \tau^{-1} \int_0^\tau P_0 dt = [(\tau + \Delta t)\tau^{-1}]^{1/2} \approx 1$, and $(\sigma_\eta^2, \sigma_v^2, \sigma_f^2, \sigma_s^2)$ are the mean-square amplitudes of $(\eta, v_r, \partial_t v_r, \partial_t \eta)$ estimated from the observational data. The function form of P_0 considers the fact that the errors of the predicted reflectivity and radial wind accumulate with time due to the equation errors of (2.1) and (2.4).

Strictly speaking, P_1 (or P_2 and P_3) should be inversely proportional to the (unknown) error variance of η (or v_r). Here it is implicitly assumed that η and v_r have about the same relative error variances, and the error variances of η and v_r are proportional to σ_η^2 and σ_v^2, respectively. Note that the residual source S' in Table 1 has about the same relative magnitude as the residual forcing F' in Table 2. This implies that the relative error for the reflectivity has the same order of magnitude as the relative error for the radial wind; that is, $O(\Delta_\eta/\sigma_\eta) \approx O(\Delta_v/\sigma_v)$. By setting $\mu_\eta = \mu_v = 1$, P_1 and P_2 are inversely proportional to σ_η^2 and σ_v^2, respectively, so J_1 and J_2 can be nearly optimally balanced in (2.7). As in XQY94a,b, $\mu = 0.01$ is used, which gives the optimal balance between J_3 and J_2 in the cost function (2.7). The values of μ_f, μ_s, k_d, k_ζ in (3.2) are properly chosen based on the results of numerical tests, although the results are not very sensitive to their variations within certain ranges (see Tables 4 and 5).

Three groups (E0–E2) of experiments are designed to test the extended methods (see Table 3). The experiments in group E0 neglect the source S_m and forcing F_m and do not use the weak divergence and vorticity constraints ($k_d = k_\zeta = 0$). The experiments in group E1 retrieve S_m and/or F_m but do not use the weak divergence and vorticity constraints. The experiments in group E2 not only retrieve S_m and/or F_m but also use the weak divergence and vorticity constraints.

Group E0 contains three experiments: experiment E0A uses the extended method A; E0B performs only the first step of method B that uses the reflectivity equation only with $P_2 = 0$ in (2.7); E0C performs only the first step of method C that uses the radial-wind equation only with $P_1 = 0$ in (2.7).

Group Ei (i = 1, 2) contains five experiments: EiA, EiB, and EiC are similar to E0A, E0B, and E0C, respectively (except for the above described differences); EiB2 and EiB3 use method B and perform two and three steps, respectively; EiC2 and EiC3 use method C and perform two and three steps, respectively.

The eight experiments in group ED (Table 4) are designed to examine the sensitivity of the retrieval to different settings of k_d and k_f. The four experiments in group EF (Table 5) are designed to examine the sensitivity of the retrieval to different settings of μ_f and μ_s.

4. Results and discussions

The results (averaged over the three datasets) of the four groups of experiments for the extended method A are summarized in Table 3, where RRE(%) represents the relative rms error of the retrieved field. In particular,

$$\mathrm{RRE}(\mathbf{v}_m) \equiv \left[\frac{\sum |\mathbf{v}_m - \mathbf{v}_{obm}|^2}{\sum |\mathbf{v}_{obm}|^2}\right]^{1/2} \tag{4.1}$$

is the relative rms error of the retrieved wind field and the summation is over the total number of 28 × 26 grid points;

$$\mathrm{RRE}(S_m) \equiv \left[\frac{\sum (S_m - S_{obm})^2}{\sum S_{obm}^2}\right]^{1/2} \tag{4.2}$$

$$\mathrm{RRE}(F_m) \equiv \left[\frac{\sum (F_m - F_{obm})^2}{\sum F_{obm}^2}\right]^{1/2} \tag{4.3}$$

are the relative rms errors of the retrieved residual source and forcing, respectively. Here S_{obm} is the observed time-mean residual source obtained by substituting the dual-Doppler observed winds and retrieved κ_η into the time-mean of (2.1), while F_{obm} is the observed time-mean residual forcing obtained by substituting the dual-Doppler observed winds and retrieved κ_v into the time mean of (2.4). The relative magnitudes of the retrieved divergence and vorticity (with respect to the observed) are listed in the last two columns of Table 4.

TABLE 4. Results of experiments ED1–ED8 (as in E2A but with variable k_d and k_f).

Experiment	k_d (s^2)	k_f (s^2)	RRE (%)	Magnitude	
			$\mathbf{v}_m$	d_m	ζ_m
ED1	0	0	36.6	2.90	2.78
ED2	10	10	33.5	2.47	1.38
ED3	50	50	28.1	1.32	1.03
ED4	100	100	25.6	1.06	0.88
ED5	200	200	25.1	0.82	0.72
ED6	500	500	23.7	0.61	0.66
ED7	750	750	23.7	0.52	0.60
ED8	1000	1000	23.8	0.47	0.59

TABLE 5. Results of experiments EF1–EF4 (as in E2B3 but with variable μ_f and μ_s).

Experiment	μ_f	μ_s	RRE (%)	
			$\mathbf{v}_m$	S_m
EF1	10^{-5}	10^{-5}	22.1	52.5
EF2	10^{-4}	10^{-4}	21.9	52.0
EF3	10^{-3}	10^{-3}	22.0	54.9
EF4	10^{-2}	10^{-2}	25.0	64.5

As shown in Table 3, the RRE in experiment E0B is smaller than in E0C. This implies that the chaff reflectivity is better conserved than the radial wind. This is indeed the case as indicated by the results in Tables 1 and 2, where the relative magnitude (43%) of the time-mean residual source term in (2.1) is smaller than the relative magnitude (56%) of the time-mean residual forcing term in (2.4). Among these three basic experiments, E0A gives the best result, so a combined use of the reflectivity and radial-wind equations can improve the retrieval. This implies that the reflectivity and radial wind measured by a Doppler radar contain independent information for the flow advection.

The results of experiments E1A, E1B, and E1C show that retrieving the time-mean residual source and/or forcing can improve the wind retrieval, though the RREs of the retrieved residual source and forcing are as large as 75%–95%. The RREs for the retrieved winds are reduced by 7.5% in E1A, by 4.2% in E1B, and by 8.2% in E1C in comparison with those in E0A, E0B, and E0C, respectively. The improvement is most significant in E1C, although experiment E1B still gives better retrievals than E1C. This result can be explained by the fact that the relative magnitude of the residual forcing (56%) in Table 2 is larger than that (43%) of the residual source in Table 1. Again, among the three experiments, the combined use of the reflectivity and radial-wind equations (E1A) gives the best result.

Experiment E1B2 performs two steps of retrieval: the first step is the same as E1B; the second step uses the first-step retrieval as the initial guess and the velocity is retrieved from the radial-wind data by using the radial-wind equation (2.4) with the forcing term F_m constrained by the estimated forcing F_{me} from the first-step retrieved velocity [see (2.9)]. As shown in Table 3, this second step improves the retrieval, but the retrieved velocity and retrieved forcing F_m in E1B2 are still not as accurate as those in E1A. The third step of retrieval is performed in E1B3, where the above second-step retrieval is used as the initial guess and the velocity is retrieved by using the reflectivity equation (2.1) with the source term S_m constrained by (2.10). With this third step, the velocity and the source term S_m retrieved in E1B3 become more accurate than those in E1A.

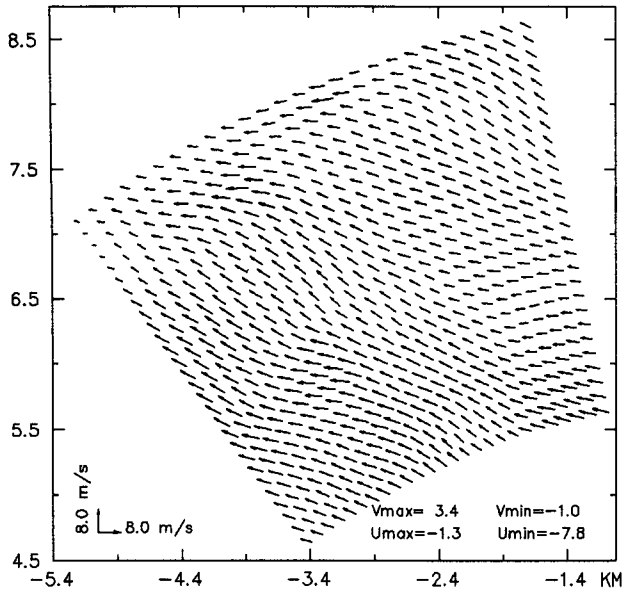

FIG. 1. Dual-Doppler observed wind field averaged over the period from the first time level to the third time level in dataset III (1237:28–1243:58 UTC 17 June 1984). The wind field is plotted over the "analysis area" in the Cartesian coordinates shown in Fig. 1 of XQY93a.

The fourth step can be performed similarly to the second step, but the retrieval cannot be significantly further improved after the third step. Similar but slightly less accurate results are obtained in the experiments (E1C2 and E1C3) with method C.

Although the results in group E1 are significantly better than in group E0, the retrieved wind fields (not shown) still contain strong divergence and vorticity, about three times as large as the dual-Doppler observed values (see ED1 in Table 4). These spuriously strong divergence and vorticity are caused mainly by short-wave noise in the data, although the data are filtered with the Cressman interpolation. To suppress the spurious divergence and vorticity, weak divergence and vorticity constraints are imposed in the experiments of group E2. These constraints clearly improve the retrievals. In comparison with those in group E1, the RREs for the retrieved winds are reduced by 11.0% in E2A, by 15.5% in E2B, by 14.3% in E2B2, by 13.7% in E2B3, by 15.1% in E2C, by 15.7% in E2C2, and by 13.4% in E2C3. The relative magnitudes of the retrieved divergence and vorticity (with respect to the observed fields) reduce to nearly unity (see ED4 in Table 4). The RREs for the retrieved residual source and/or forcing are also reduced (see Table 3).

In group E2, the velocity field can be quite accurately retrieved even in the first step of E2B (or E2C), so the forcing (or source) term can be quite accurately estimated in the second step of E2B2 (or E2C2). This and the fact that the radial-wind (or reflectivity) information used in the second-step retrieval is independent of the reflectivity (or radial wind) information used to estimate the forcing (or source) may explain why the retrieval in E2B2 (or E2C2) is slightly more accurate than the combined retrieval in E2A. The retrieval is further improved by the third step in E2B3 or E2C3. Again, the results with method C are slightly less accurate than those with method B, and the reason is that method B uses the reflectivity equation first and the chaff reflectivity is better conserved than the radial wind in the Phoenix II data.

The retrieved wind fields (from dataset III) are shown in Figs. 2–5 for E2C, E2B, E2A, and E2B3. Although the four retrieved wind fields are all quite close to the dual-Doppler observed wind field (Fig. 1), the improvements in the retrieved wind fields from Fig. 2 (E2C) to Fig. 3 (E2B), to Fig. 4 (E2A), and finally to Fig. 5 (E2B3) are notable. The retrieval reaches the best accuracy at the third step in E2B3 and cannot be further improved in the fourth and fifth steps. By the third step, both the reflectivity data and radial-wind data have been used to estimate the forcing and source terms, so after the third step the estimated forcing and source terms will be hardly further improved. This explains why three steps will suffice.

The eight experiments in group ED (Table 4) are similar to E2A (in Table 3) but with different settings of k_d and k_ζ. As shown in Table 4, when k_d and k_ζ are between 50 and 200 s^2, the spurious divergence and vorticity are optimally suppressed. When k_d and k_ζ are between 500 and 700 s^2, the RRE of the retrieved wind field reaches the minimum, but the retrieved divergence and vorticity are overly suppressed and become significantly weaker than their respective true magnitudes

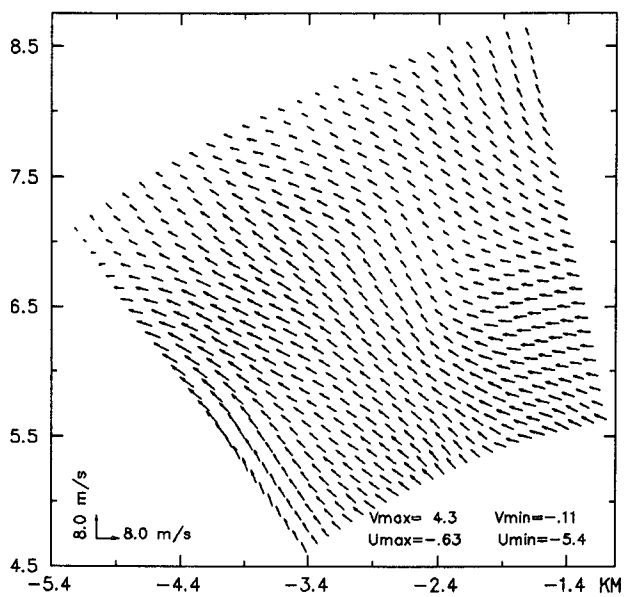

FIG. 2. Retrieved wind field in experiment E2C with dataset III. The rms error and RRE of the retrieved winds are 1.74 m s^{-1} and 36.8%, respectively.

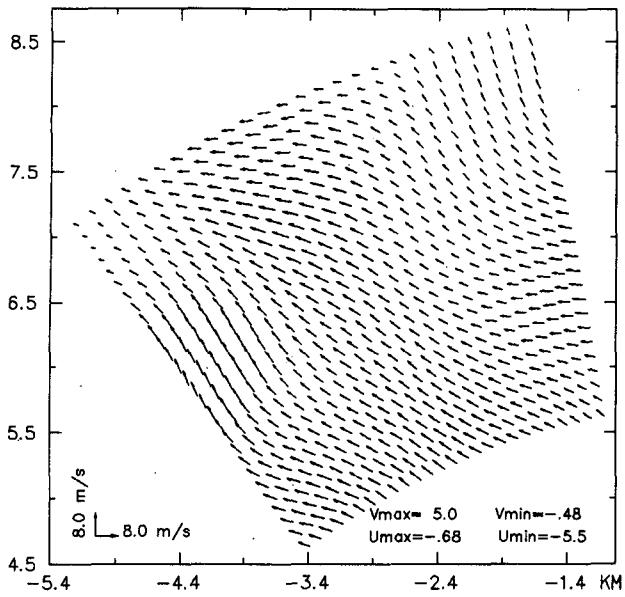

FIG. 3. As in Fig. 2 but for experiment E2B. The rms error and RRE are 1.57 m s^{-1} and 33.2%, respectively.

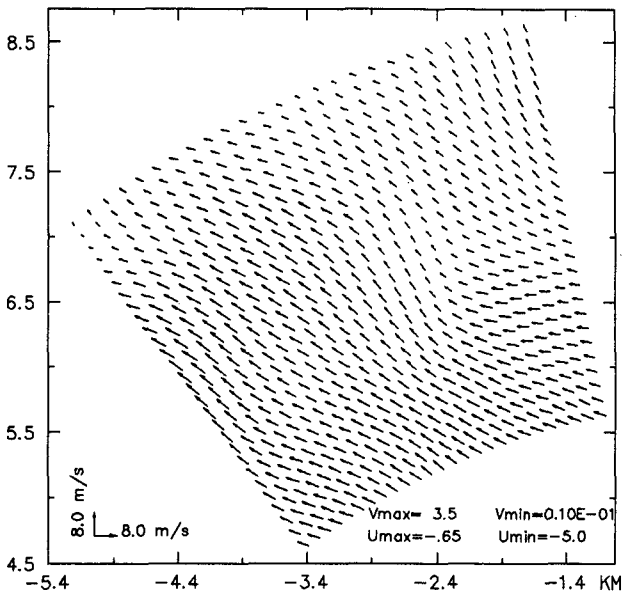

FIG. 4. As in Fig. 2 but for experiment E2A. The rms error and RRE are 1.45 m s^{-1} and 30.7%, respectively.

(as observed by the dual-Doppler radars). Note that the RREs of the retrieved winds remain relatively small and insensitive to the settings of k_d and k_f between 50 and 1000 s^2.

The four experiments in group EF (Table 5) are similar to E2B3 in Table 3 but with different settings of μ_f and μ_s. This group of experiments examines the sensitivity of the retrieval to different settings of μ_f and μ_s. As shown in Table 5, the best retrieval is given by $\mu_f = \mu_s = 10^{-4}$ in EF2, and RREs of the retrieved winds remain small and insensitive to the settings of μ_f and μ_s over the wide range from 10^{-5} to 10^{-3}.

5. Conclusions

In this paper, the simple adjoint (SA) method of QX92 is extended and tested with the Phoenix II data for retrieving the low-altitude winds from the movements of reflectivity patterns and radial-wind patterns measured through a sequence of single-Doppler radar scans. The SA method was previously upgraded and tested for retrieving the low-altitude winds either from the movements of reflectivity patterns by using the reflectivity equation (XQY94a) or from the movements of radial-wind patterns by using the radial-wind equation (XQY94b), but a combined use of the two equations was not explored. Since the reflectivity and radial wind measured by a Doppler radar contain independent information for the flow advection, a combined use of the two equations may improve the velocity retrieval and make the retrieval more reliable. To achieve this, three extended methods are proposed and tested with the Doppler radar data measured during the Phoenix II field experiment. The extended method A uses the reflectivity equation and radial-wind equation simultaneously. The extended method B (or method C) uses the reflectivity equation and radial-wind equation alternately with the reflectivity equation (or radial-wind equation) used in the first step, then the retrieved velocity is substituted into the radial-wind (or reflectivity) equation to estimate the forcing (or source) term for the next step of retrieval. All the three extended

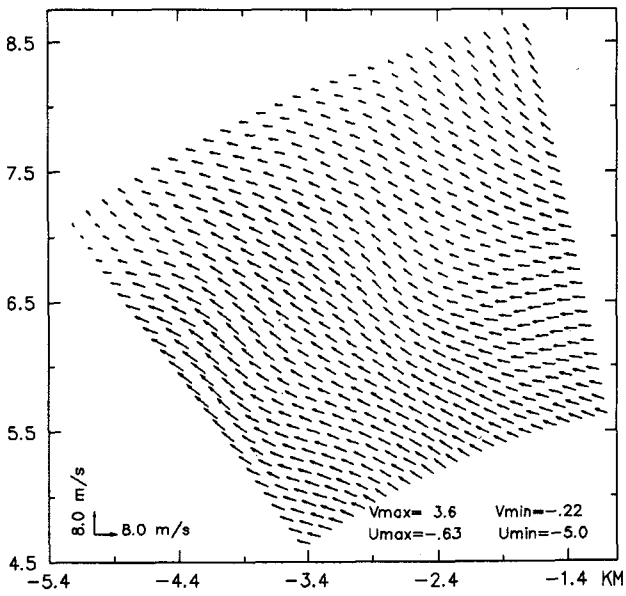

FIG. 5. As in Fig. 2 but for experiment E2B3. The rms error and RRE are 1.16 m s^{-1} and 24.6%, respectively.

methods improved the retrievals obtained by the previous SA method based on a single (reflectivity or radial wind) equation. Among the three extended methods, method C is found to be slightly better than method A, slightly worse than method B, and the reason is due to the fact that the chaff reflectivity is better conserved than the radial wind in the Phoenix II data.

Although only a limited number of experiments are presented and compared in this paper, the extended methods have been tested with additional experiments on different aspects, as in QX92 and XQY94a. The test results confirm the basic merit of the SA method obtained in QX92 and also support the detailed techniques developed in XQY94a,b. In addition to the previous findings, this paper shows that (i) a properly weighted combined use of the reflectivity data and radial-wind data can improve the retrieval, (ii) retrieving the time-mean residual source term (in addition to the time-mean residual forcing term) improves the wind retrieval, (iii) imposing a weak vorticity constraint (in addition to the weak divergence constraint) can also improve the retrieval, and (iv) the retrievals are not sensitive to the weights in the weak vorticity and divergence constraints [see (2.7), (3.2), and Table 4] and insensitive to the weights in the weak constraints imposed by the estimated forcing and source in method B and method C [see (2.9), (2.10), (3.2), and Table 5]. These insensitivities are useful for operational applications of the method, in which case the weights cannot be optimally adjusted from case to case due to the lack of a prior knowledge of the wind field, but nearly optimal retrievals still can be obtained with properly fixed weights.

Finally, it is necessary to point out that a combined use of the reflectivity data and radial-wind data may not always improve the retrieval, especially when the data and equation errors for reflectivity (or radial wind) are substantially larger than for radial wind (or reflectivity). This may pose a limitation for a combined use of storm reflectivity data and radial-wind data, because hydrometeor reflectivity is conserved to a much lesser extent than chaff reflectivity and the equation error represented by the temporal fluctuation of the reflectivity source may be considerably large. To improve the wind retrieval through a combined use of storm reflectivity and radial-wind data, the hydrometeor reflectivity source may need to be better estimated, perhaps, with additional physical constraints and data information. This problem needs further investigation.

Acknowledgments. We are grateful to R. Kropfli, H. Gu, and J.-X. Yu for their help in many aspects and are thankful to A. Shapiro, D. K. Lilly, J. Doviak, D. Zrnić, and anonymous reviewers for their comments and suggestions. Phoenix II data were kindly provided by R. Kropfli at NOAA/ETL and J. Schneider at NOAA/NSSL. This work is supported by the NOAA Grant NA37RJ0203, the DOE ARM Program through Battelle PNL Contract 144880-A-Q1 to CIMMS, and by NSF Grant ATM91-20009 and FAA contract to CAPS, the University of Oklahoma.

REFERENCES

Lewis, J. M., and J. C. Derber, 1985: The use of adjoint equations to solve a variational adjustment problem with advective constraints. *Tellus,* **37A,** 309–322.

Moore, A. M., 1991: Data assimilation in a quasigeostrophic open-ocean model of the Gulf Stream region using the adjoint method. *J. Phys. Oceanogr.,* **21,** 398–427.

Qiu, C. J., and Q. Xu, 1992: A simple adjoint method of wind analysis for single-Doppler data. *J. Atmos. Oceanic Technol.,* **9,** 588–598.

Sasaki, Y. K., 1970: Some basic formalisms in numerical variational analysis. *Mon. Wea. Rev.,* **98,** 875–883.

Talagrand, O., and P. Courtier, 1987: Variational assimilation of meteorological observation with the adjoint vorticity equation. Part 1: Theory. *Quart. J. Roy. Meteor. Soc.,* **113,** 1311–1328.

Xu, Q., and C. J. Qiu, 1994: Simple adjoint methods for single-Doppler wind analysis with a strong constraint of mass conservation. *J. Atmos. Oceanic Technol.,* **11,** 289–298.

——, ——, and J. X. Yu, 1994a: Adjoint-method retrievals of low-altitude wind fields from single-Doppler reflectivity measured during Phoenix II. *J. Atmos. Oceanic Technol.,* **11,** 275–288.

——, ——, and ——, 1994b: Adjoint-method retrievals of low-altitude wind fields from single-Doppler wind data. *J. Atmos. Oceanic Technol.,* **11,** 579–585.